High-resolution Compton scattering study of the electron momentum density in Al

T. Ohata and M. Itou
Japan Synchrotron Radiation Research Institute, Kamigouri, Akougun, Hyogo 678-12, Japan

I. Matsumoto
Department of Synchrotron Radiation Science, Graduate University for Advanced Studies, Tsukuba 305, Japan

Y. Sakurai
Japan Synchrotron Radiation Research Institute, Kamigouri, Akougun, Hyogo 678-12, Japan

H. Kawata
Institute of Materials Structure Science, High Energy Accelerator Research Organization, Tsukuba, Ibaraki 305, Japan

N. Shiotani
Tokyo University of Fisheries, Kounan, Minato, Tokyo 108, Japan

S. Kaprzyk
Academy of Mining and Metallurgy, aleja Mickiewicza 30, PL-30-059 Krakow, Poland
and Department of Physics, Northeastern University, Boston, Massachusetts 02115

P. E. Mijnarends
Department of Physics, Northeastern University, Boston, Massachusetts 02115
and Interfaculty Reactor Institute, Delft University of Technology, 2629 JB Delft, The Netherlands

A. Bansil
Department of Physics, Northeastern University, Boston, Massachusetts 02115
(Received 12 May 2000)

We report high-resolution Compton profiles (CP's) of Al along the three principal symmetry directions at a photon energy of 59.38 keV, together with corresponding highly accurate theoretical profiles obtained within the local-density approximation (LDA) based band-theory framework. A good accord between theory and experiment is found with respect to the overall shapes of the CP's and their first and second derivatives, as well as the anisotropies in the CP's defined as differences between pairs of various CP's. There are, however, discrepancies in that, in comparison to the LDA predictions, the measured profiles are lower at low momenta, show a Fermi cutoff that is broader, and display a tail that is higher at momenta above the Fermi momentum. A number of simple model calculations are carried out in order to gain insight into the nature of the underlying 3D momentum density in Al and the role of the Fermi surface in inducing fine structure in the CP's. The present results when compared with those on Li show clearly that the size of discrepancies between theoretical and experimental CP's is markedly smaller in Al than in Li. This indicates that, with increasing electron density, the conventional picture of the electron gas becomes more representative of the momentum density and that shortcomings of the LDA framework in describing the electron correlation effects become less important.

I. INTRODUCTION

In a Compton scattering experiment one measures the so-called Compton profile (CP),

$$J(p_z)=\int\int \rho(\mathbf{p})dp_x dp_y, \tag{1}$$

where $\rho(\mathbf{p})$ is the ground-state electron momentum density. In an independent-particle model the momentum density is given by

$$\rho(\mathbf{p})=(2\pi)^{-3}\sum\left|\int \psi(\mathbf{r})\exp(i\mathbf{p}\cdot\mathbf{r})d\mathbf{r}\right|^2, \tag{2}$$

where $\psi(\mathbf{r})$ denotes the electron wave function.[1–4] The summation in Eq. (2) extends over all occupied states. The Compton profile, $J(p_z)$, thus contains signatures of the Fermi surface breaks and correlation effects in the underlying three-dimensional momentum distribution $\rho(\mathbf{p})$. Since Fermi momenta p_F are typically ~ 1 a.u., a high momentum resolution of ~ 0.1 a.u. is essential in the experiment for delineating Fermi-surface-related fine structure in the CP.

High-resolution Compton studies have recently been reported on Li,[5,6] Be,[7–9] V,[10] and Cu.[11] In all these cases, careful comparisons of the shapes of the absolute valence electron CP's, and the structure in the first and second derivatives as well as the directional anisotropies of the

CP's, have been made with the corresponding parameter-free theoretical predictions based on the use of the local-density approximation (LDA). A similar investigation of Li-rich LiMg disordered alloys where disorder effects were treated using the mean-field Korringa-Kohn-Rostoker (KKR) coherent potential approximation (CPA) approach has also been carried out.[12] In this way, the band-theory-based LDA approach has been shown to provide a remarkably accurate description of many aspects of the momentum density associated with the quantum-mechanical electronic ground state, including the characteristic fine structure induced by the Fermi surface. More exciting, however, is the fact that the aforementioned comparisons have clearly established the presence of systematic deviations between theoretical and experimental momentum densities. In Li, the experimental break Z_k in the momentum density at p_F appears to be very small, nearly zero;[6] if so, this is very far from the results of electron gas calculations stretching over the last several decades.[13] In Be, the latest Compton data[9] indicate *anisotropic* electron correlation effects outside the scope of much of the existing theoretical work that is based on treating properties of the homogeneous electron gas.[14–19] For these reasons, a renewed interest in the problem of correlation effects on the momentum density beyond the LDA is natural,[20–24] although much further work is necessary for developing an approach of wide applicability in metals and alloys.

Bearing these considerations in mind, there is strong motivation for undertaking high-resolution Compton studies of other systems. Our choice of Al in this connection is an especially good one because Al is trivalent and, therefore, it extends the range of electron densities investigated so far via high-resolution Compton scattering. Correlation effects are of course expected to become less important with increasing electron density as the kinetic energy dominates. Also, Al has been the traditional touchstone of a free-electron-like metal with a nearly spherical Fermi surface (viewed in the extended zone). Neither a high-resolution, high-statistics Compton measurement nor a band-theory computation of high accuracy in order to identify Fermi-surface-related fine structure in the CP's of Al is currently available in the literature.[25,26] The goal of the present work is to fill this gap and determine the extent to which the LDA describes the momentum density in Al. The existing Compton data on Al consists essentially of a number of measured CP's using γ-ray sources and solid-state detectors at low momentum resolution.[27–30] Quite some time ago, Shiotani *et al.*[31] obtained the [111] CP of Al at a momentum resolution of 0.08 a.u., but did not investigate the anisotropy of the CP or the Fermi-surface signatures therein.

An outline of this article is as follows. In the next section we describe the experimental procedures. Section III gives pertinent details of computations. In Sec. IV the experimental CP's are analyzed in the light of band-theory predictions as well as a number of other model computations. The Compton results are also compared briefly with closely related positron-annihilation spectra. Section V summarizes our main conclusions.

II. EXPERIMENT

Single crystals of Al with surface normals oriented along the [100], [110], and [111] directions were used. The thickness of the crystals was about 2 mm. The reader is referred to Sakurai *et al.*[32] for details of our Compton spectrometer, and to Tanaka *et al.*[33] and Itou *et al.*[8] for our data processing procedures. Briefly, the spectrometer consists of a Cauchois-type bent-crystal analyzer of Si(422) with an image plate serving as a position-sensitive detector. The scattering angle is 160°. The synchrotron radiation x rays from a multipole wiggler installed in the 6.5 GeV Accumulation Ring at the National Laboratory for High Energy Physics are monochromatized by a quasi-doubly-bent monochromator to 59.38 keV with an energy resolution of about 80 eV. The overall momentum resolution is estimated to be 0.12 a.u. The double-Compton-scattering events were simulated via the Monte Carlo program of Sakai;[34] the integrated intensity of the double-scattering events was found to be 10% of the single-scattering events.

The statistical error of each datum point, given by $\sigma = \sqrt{N} + 0.003N$, is estimated to be less than 0.3%. Since the data points are not measured equidistantly they are interpolated onto an equidistant mesh of 0.02 a.u. using simple linear interpolation. The data were numerically differentiated according to $y'(i) = \frac{1}{2}\{[y(i+1)-y(i)]/[x(i+1)-x(i)] + [y(i)-y(i-1)]/[x(i)-x(i-1)]\}$. No further smoothing or filtering was applied. The interpolation and differentiation cause some statistical correlation between the data points.

III. COMPUTATIONS

The band-structure problem was solved within the all-electron charge self-consistent KKR framework without any free parameter. Exchange-correlation effects were incorporated using the von Barth–Hedin local-spin-density (LSD) approximation.[35] The lattice constant was computed to be 7.6534 a.u. by minimizing the total energy; for comparison, the experimental lattice constant at room temperature is 7.6559 a.u. The self-consistent crystal potential was obtained by iterating the KKR cycles using an elliptic contour with 48 points in the complex energy plane. The final charge density is self-consistent to an accuracy of about 10^{-4} electrons and the Fermi energy to 10^{-4} Ry. An angular momentum cutoff $l_{max}=2$ was employed. A free-electron-like Fermi surface was found with Fermi radii $k_{100}=0.9246$, $k_{110}=0.9255$, and $k_{111}=0.9292$ a.u.; the free-electron value would be 0.9254 a.u.

The CP's were obtained by first evaluating the three-dimensional momentum density $\rho(\mathbf{p})$ in terms of the momentum matrix element of the KKR Green's function[36–39] over a fine mesh of $48\times4851\times177$ $\mathbf{p}$ points, covering momenta up to $p_{max}\sim5$ a.u. This mesh involves 4851 $\mathbf{k}$ points in the 1/48th irreducible part of the Brillouin zone with each $\mathbf{k}$- point translated into 177 $\mathbf{p}$ points by adding reciprocal lattice vectors; the factor of 48 takes into account the symmetry operations of the cubic point group. The CP's can then be computed accurately by evaluating the two-dimensional integral of Eq. (1) using a generalized linear tetrahedron method.[40] The final CP's have been calculated over a momentum mesh containing 151 p_z points in the range 0–3 a.u. along each of the three measured directions. The accuracy of the computed profiles is about 1 part in 10^4. A similar integration technique has been used in our earlier studies of high-resolution CP's of various metals and

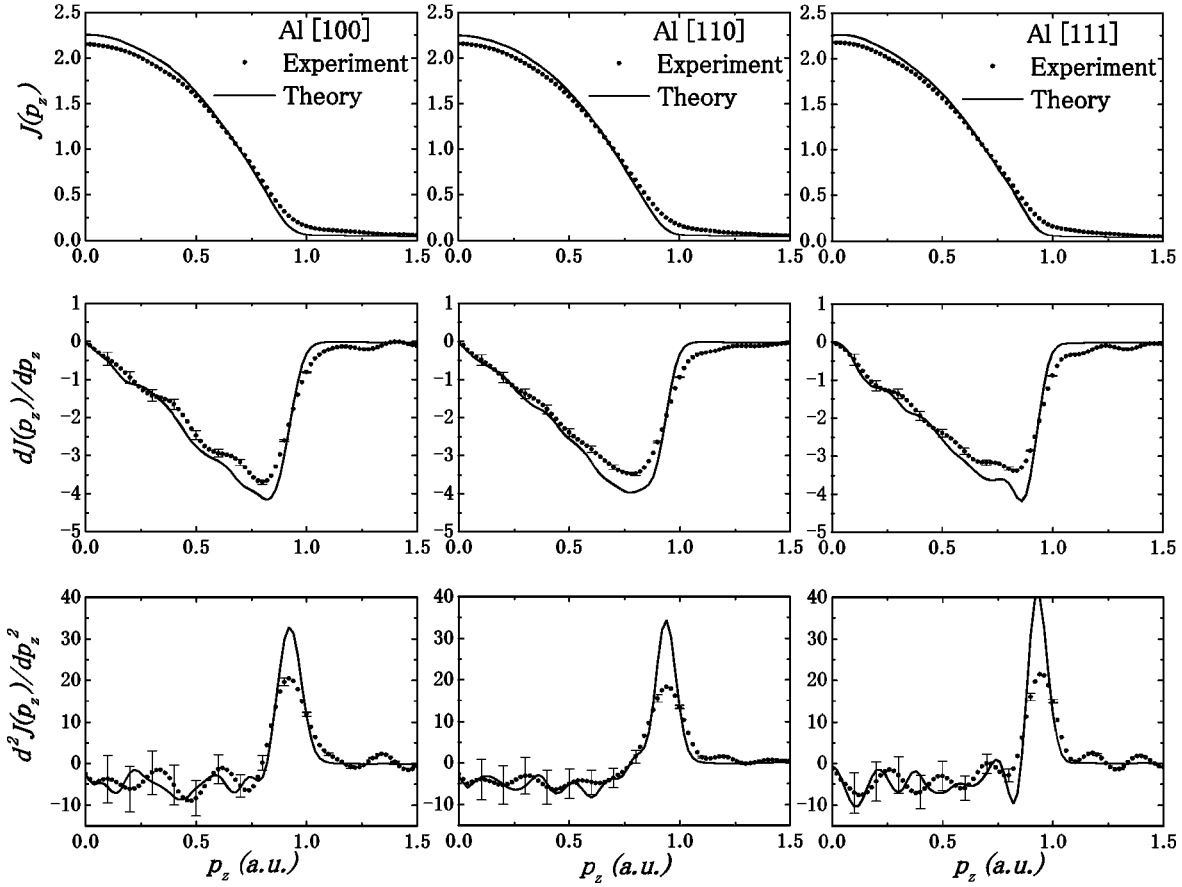

FIG. 1. Top: Measured and computed Compton profiles of Al along the [100], [110], and [111] directions. Theoretical profiles (solid lines) have been broadened to reflect experimental resolution. Middle: First derivatives of the measured and computed profiles. Bottom: Second derivatives of the measured and the computed profiles.

alloys.[5,7–9,11,26,41,42] The Lam-Platzman correction[43] to the CP's was computed using the occupation number density of the uniform electron gas.

IV. RESULTS AND DISCUSSION

Figure 1 shows the measured and computed CP's of the valence electrons along the [100], [110], and [111] directions; the theoretical CP's are convoluted with a Gaussian that represents the experimental resolution of 0.12 a.u. full width at half maximum (FWHM). The experimental valence CP's have been obtained by subtracting the theoretical core CP's from the measured profiles. In this connection, we used the solid-state core wave functions that reflect the slight overlap of the $2p$ core states in Al. The first and second derivatives of the valence profiles have been obtained by numerical differentiation.

In examining the overall shape of the CP's in Fig. 1, one notes that the experimental points are lower at low momenta compared to the calculated values. We emphasize that this does not imply that the measured 3D momentum density is lower than the theoretical one at all momenta. To see this, recall that[44]

$$\rho(0) = -\frac{1}{2\pi}\frac{d^2 J_{\mathrm{av}}(p)}{dp^2}\bigg|_{p=0}, \tag{3}$$

where $J_{av}(p)$ denotes the directionally averaged CP, which in a cubic crystal may be reasonably approximated by[45]

$$J_{\mathrm{av}}(p) = (1/35)[10J_{100}(p) + 16J_{110}(p) + 9J_{111}(p)]. \tag{4}$$

The bottom row in Fig. 1 shows that the differences between the experimental and theoretical second derivatives at $p_z = 0$ are well within the error bars. In view of Eq. (3), this indicates that the underlying 3D distributions are not significantly different at $p_z = 0$. In fact, this result implies that the measured momentum density must be smaller than the theoretical one at momenta approaching the Fermi momentum p_f. This is also borne out by the first derivatives shown in the central row of Fig. 1, which begin to show differences between experiment and theory only above $p_z \sim 0.3$ a.u.

Further insight is provided by Fig. 2, which shows the spherically averaged 3D momentum density defined by

$$\rho_{\mathrm{av}}(p) = -(1/2\pi p)(dJ_{\mathrm{av}}/dp), \tag{5}$$

where $J_{\mathrm{av}}(p)$ is obtained via Eq. (4). The oscillations in $\rho_{\mathrm{av}}(p)$ at small momenta reflect partly the large (correlated) error bars due to the division of the small derivative by small values of p, and partly the (spherically averaged) effect of Brillouin-zone-face interactions to be discussed below. In any event, Fig. 2 makes it clear that the experimental 3D momentum density lies below the theoretical predictions as one approaches p_F and that the situation reverses itself above p_F.

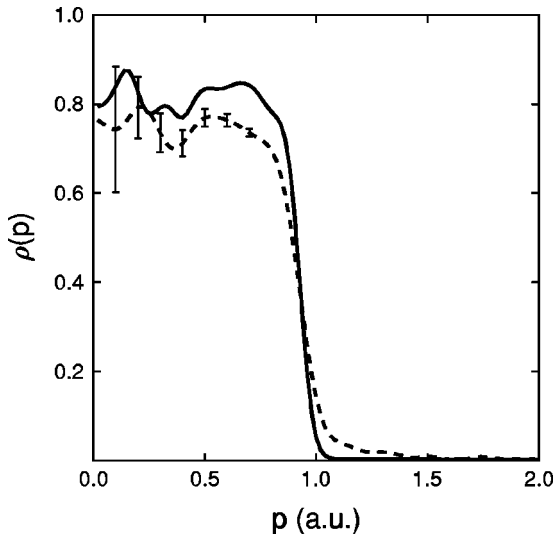

FIG. 2. Theoretical (solid curve) and experimental (dashed curve) directionally averaged 3D electron momentum density obtained via Eqs. (4) and (5).

The second derivatives J'' in Fig. 1 all show a peak at p_F. There is good agreement between theory and experiment as to the position of the peaks, i.e., the value of p_F, but the measured peaks are all lower and broader than the theoretical predictions. Although the shapes of the J'' peaks reflect the complex interplay between the effects of experimental resolution, electron correlations, and lattice potential on the Fermi cutoff in the momentum density, it is evident from Figs. 1 and 2 that the measured distribution possesses a tail higher than the theory beyond p_F.

These discrepancies between theory and experiment are similar to those reported earlier in Li (Refs. 5 and 6) and other metals (Refs. 7–9 and 11) and have their origin in the electron correlation effects beyond the LDA, which are not treated properly within our theoretical framework. Such correlations are expected to cause (relative to the independent-particle model) a decrease of the momentum density as one approaches p_F and a tail at momenta greater than p_F; as indicated above, both features are qualitatively visible in our comparison between theory and experiment. Notably, the deviations from LDA theory are smaller in Al than in Li. For example, the difference between the theoretical and experimental valence profiles at $p_z=0$ is approximately 16% for Li and 4.5% for Al,[46] and the width of the peak at p_F in the second derivatives is 0.23 a.u. in Li and 0.15 a.u. in Al; thus, the ''blurring'' of the Fermi cutoff is more severe in Li than in Al. These characteristic differences between Li and Al are partly related to the difference in the electron density of the two metals. The electron density in terms of r_s (the standard parameter for the volume per electron of valence electrons), is 3.21 for Li and 2.12 for Al. Therefore, the bare Coulomb interaction is more effectively screened in Al than in Li. As shown by a variety of treatments of the homogeneous interacting electron gas, as the electron density increases, the kinetic energy dominates, and the momentum density is described more closely by the free-electron rectangular distribution with a stepwise cutoff at p_F.[14–19,47–49]

Figure 3 considers the effect of the isotropic Lam-Platzman (LP) correction on the [111] CP; results along

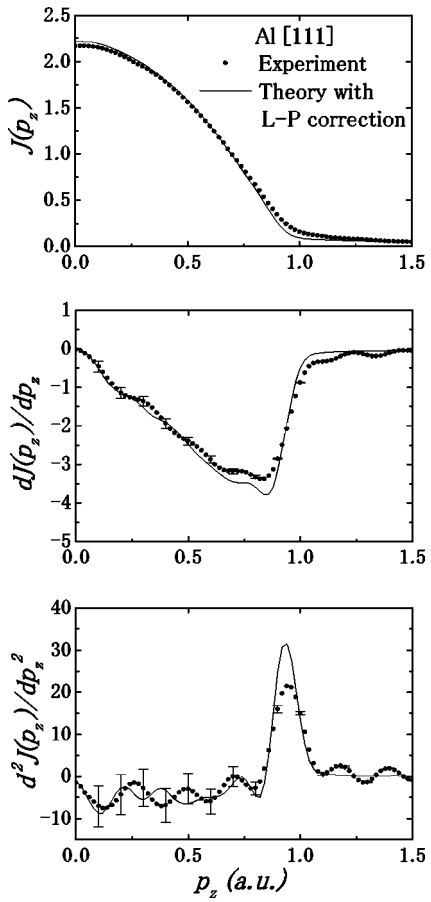

FIG. 3. Same as the last column of Fig. 1, except that here the theoretical curves in all cases include the Lam-Platzman correction.

other directions are similar and are not shown in the interest of brevity. The theoretical curves in Fig. 3 include the LP correction, while those in Fig. 1 do not. A comparison of Fig. 3 with the last column of Fig. 1 shows that, although the inclusion of the LP correction improves things, much of the discrepancy between theory and experiment still remains. Interestingly, Suortti *et al.*[26] have recently analyzed the correlation correction to the CP's of Al in terms of a model that involves the break Z_k in the momentum density at p_F as the only free parameter. By adjusting Z_k, Suortti *et al.*[26] find that the discrepancy between the LDA predictions and the measurements can be essentially removed for a Z_k value between 0.7 and 0.8, in reasonable accord with the corresponding theoretical values from various authors that are scattered between 0.76 and 0.85.[14–19] There is no inconsistency between the present results and those of Ref. 26. To see this relationship, recall that the standard LP correction is defined via[43]

$$\Delta\rho(p)=\int d^3r\,\rho(\mathbf{r})[\rho^{INT}(p,r_s(\mathbf{r}))-\rho^{NI}(p,r_s(\mathbf{r}))], \quad (6)$$

where the integral extends over the Wigner-Seitz cell. The expression within the square brackets gives the difference between the momentum densities of the interacting and noninteracting *homogeneous* electron gas (denoted by the superscripts INT and NI) evaluated at the local density $\rho(\mathbf{r})$ of the physical system, and $r_s(\mathbf{r})$ is the corresponding electron density parameter. Equation (6) thus attempts to take into ac-

count inhomogeneities in the electron gas, whereas the semiempirical model of Ref. 26 replaces the integrand by its value at the average electron density in Al. The matter is quite subtle, and further work is necessary in order to develop a satisfactory treatment of correlation effects on the momentum density in solids.

If the momentum density within the Fermi sphere were flat and smooth, the first derivative $dJ(p_z)/dp_z$ shown in the middle row of Fig. 1 would be a straight line up to the cutoff at the Fermi momentum. However, at momenta less than the Fermi radius some structure is visible notably in the [111] and the [100] derivatives. In this connection, we note that the Fermi sphere overlaps with umklapp Fermi spheres centered on the (111) reciprocal lattice points around the *W* points in the Brillouin zone. For example, the hexagonal zone face contains six *W* points that all project at $(\frac{1}{2},\frac{1}{2},\frac{1}{2})$, i.e., the point $p_z=0.71$ a.u. on the [111] axis. Similarly, four *W* points in the first Brillouin zone project at 0.41 a.u. and another four at 0.82 a.u. on the [100] direction. Interestingly, the experimental as well as the theoretical derivatives contain structure around 0.7 a.u. in the [111] and 0.4 a.u. in the [100] CP. This indicates the importance of the k states near the *W* points with respect to the fine structure in the Al CP's. Incidentally, a structure similar to the wiggle around 0.4 a.u. in the [100] derivative has been observed in positron-annihilation 1D ACAR measurements by Okada *et al.*[50] and 2D ACAR measurements by Mader *et al.*,[51] who also ascribed it to zone-face interactions around the *W* points.

The directional differences, shown in Fig. 4, are a measure of the anisotropy. Although the maximum difference is about 1% of the peak value of the profile itself, they show definite structures that can have several origins. First, for different crystal orientations the plane of integration in Eq. (1) sweeps differently through the umklapp Fermi spheres centered at the reciprocal lattice points in the higher Brillouin zones. Second, the Fermi surface is slightly distorted from a sphere, as witnessed by the different Fermi radii given above, while, third, band-structure effects such as a **p** dependence of the momentum density within the Fermi spheres and interactions of the electron bands with the Brillouin-zone faces with consequent distortion of the wave functions will also contribute to the anisotropy. The importance of the first point can be readily studied using a simple model of a spherical free-electron-like Fermi surface surrounded by seven shells of similar umklapp Fermi surfaces. The momentum density within each Fermi surface is assumed to be constant and given by the square of the corresponding Fourier component of the electron wave function at Γ_1.[3] The CP for a given direction then consists of a superposition of inverted parabolas, centered at the projections on that direction of the reciprocal lattice points. The height of each parabola is proportional to the momentum density within the corresponding Fermi sphere, while its cutoff points are found by adding or subtracting p_F from the projected center. Figure 5 shows the directional differences thus obtained. The positions of the cutoff points have been indicated by the arrows at the bottom of the graph, together with a symbol that denotes the direction of projection ($a=[100], b=[110], c=[111]$) and the coordinates of the center of the Fermi sphere. It should be noted that many umklapp Fermi spheres coincide in projection and therefore

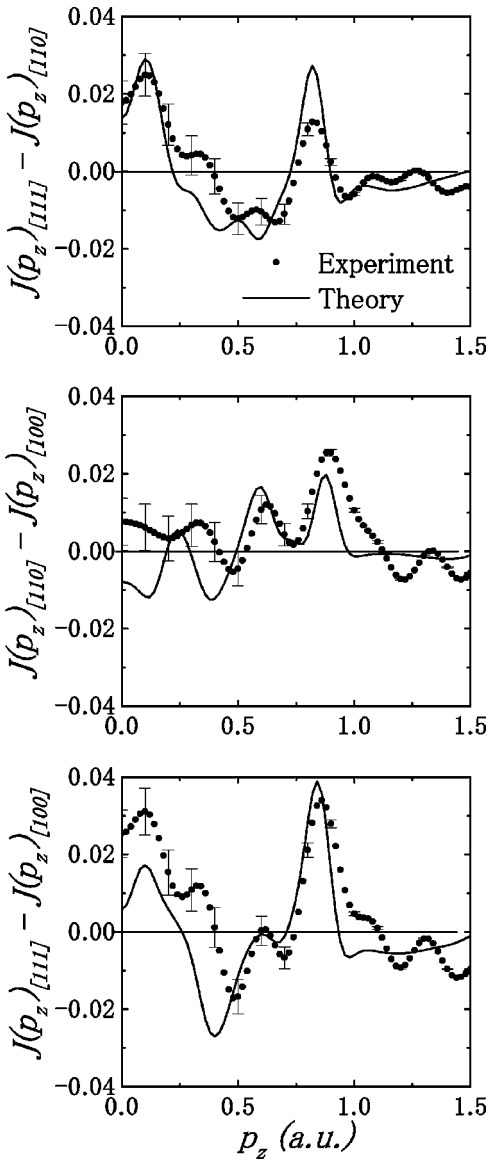

FIG. 4. Measured and computed directional difference profiles for three different pairs of directions.

these coordinates are not unique; the simplest set has been noted. The analysis in Fig. 5 shows that much of the important structure in the directional differences stems from the ⟨111⟩ umklapp contributions; the other umklapp contributions play a less important role.

A comparison of Fig. 5 with the calculated differences in Fig. 4 shows an overall qualitative correspondence in the succession of positive and negative peaks. On a more detailed scale, however, there are significant differences that have their origin in the other factors mentioned above. Notable examples are the peaks around 0.85 a.u. in the $J_{[111]}-J_{[100]}$ and $J_{[111]}-J_{[110]}$ directional differences in Fig. 4 that have no clear counterpart in Fig. 5. Kubo *et al.*[52] have ascribed these features to the fact that in the [111] direction the actual Fermi surface bulges out beyond the free-electron Fermi sphere in the second Brillouin zone while there is a contraction in the third zone. This will strongly affect the [111] profile but not so much the other two. Our simple free-electron model of course does not contain this Fermi-surface distortion effect. The calculated curves in Fig. 4, on

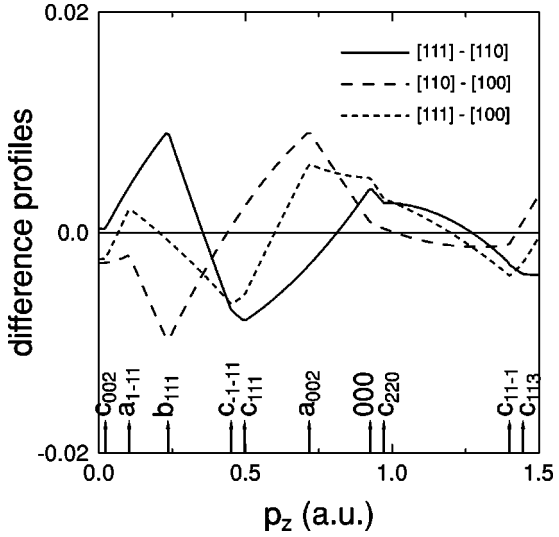

FIG. 5. Directional difference profiles calculated for a simple quasi-free-electron model of Al in which the CP is given by a superposition of parabolic contributions centered at various reciprocal lattice points (see text). The arrows at the bottom indicate the positions of the cutoff points (each parabola has two cutoff points; the other one lies outside the graph). The directions of projection are indicated by a (=[100]), b (=[110]), and c (=[111]), while the subscripts denote the coordinates of the reciprocal lattice points involved. 000 denotes the cutoff of the central Fermi surface, i.e., the Fermi radius p_F.

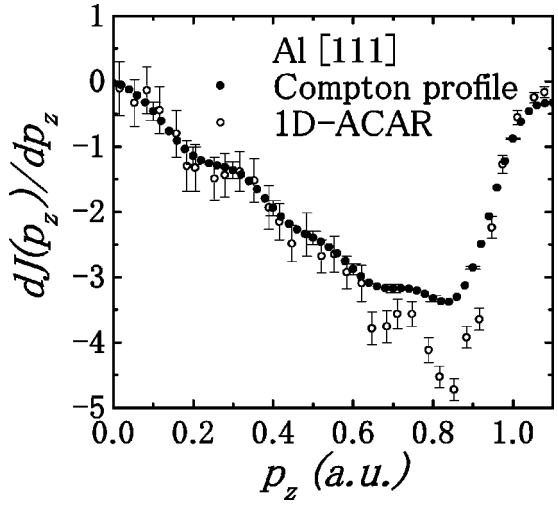

FIG. 6. First derivative of the 1D ACAR spectrum (open circles) along the [111] direction read off from Ref. 50 is compared with the derivative of the [111] Compton profile shown in Fig. 1.

the other hand, include all of these factors and reproduce the essential characteristics of the measured differences, although some discrepancies remain. It may be noted that nonlocality of the exchange and correlation potential in Li reduces the Fermi-surface anisotropy[53,54] and thus would affect the anisotropy of the CP's. In this vein, lattice vibrations would reduce the umklapp contributions and hence the anisotropy of the momentum density. How far such effects can explain the residual discrepancies in Fig. 4 remains unclear.

In principle, the anisotropy in the momentum density may be obtained approximately by expanding both the momentum density and the CP's into lattice harmonics and establishing the relation between the expansion coefficients for the momentum density and those for the CP's.[55] Actually, Eq. (5) represents the $l=0$ term in such a scheme. However, we have not attempted to analyze our data along these lines since the number of measured profiles is not large enough.

Additional information may be gained from a comparison of CP's with the corresponding results of positron annihilation measurements. Both experiments probe the momentum density—in positron annihilation one measures the momentum density of the annihilating electron-positron pair whereas in Compton experiment only the electron momentum density is involved. In Fig. 6 the first derivative of the one-dimensional angular correlation of positron-annihilation radiation (1D ACAR) profile measured by Okada *et al.*[50] for the [111] orientation is compared with the corresponding CP. The momentum resolution of the 1D ACAR profile is 0.11 a.u., which is almost the same as that of the present CP's. Since the 1D ACAR profile was area normalized to the theoretical 1D ACAR profile calculated by Kubo *et al.*,[52] the peak height at $p_z=0$ is almost the same as that of the present CP. The slope at the Fermi momentum is steeper in the 1D ACAR profile than in the CP, which is direct evidence for enhancement of the annihilation of positrons with the *s-p* electrons near the Fermi energy predicted first by Kahana[56] on the basis of an interacting electron gas model. Also, the correlation tail for $p>p_F$ in the 1D ACAR profile is weaker than its counterpart in the CP as a result of the partial cancellation of electron-electron and positron-electron correlation effects.[57] Finally, the fine structure at 0.2 a.u. and 0.7 a.u. is more pronounced in the 1D ACAR profile than in the CP. This points to less correlation-induced smearing in positron annihilation compared to Compton scattering.

V. SUMMARY AND CONCLUSIONS

We have measured the Compton profiles (CP's) of Al along [100], [110], and [111] directions at a photon energy of 59.38 keV and a momentum resolution of 0.12 a.u. Parallel, highly accurate all-electron computations have been carried out within the LDA-based band-theory framework. Comparisons between theory and experiment at the level of the shapes of the CP's, structure in the first and second derivatives of the CP's, and anisotropies obtained by taking differences between three pairs of CP's all show a good level of accord. However, there are discrepancies as well. In comparison to the LDA predictions, the measured profiles are lower at low momenta, show a Fermi cutoff that is broader, and display a tail that is higher at momenta above the Fermi momentum. The inclusion of correlation effects in the LDA via the standard isotropic Lam-Platzman correction improves the comparison slightly, but the essential discrepancies remain. A model analysis in terms of directionally averaged CP's allows us to determine on the 3D momentum density of Al; in this way, we adduce that the experimental 3D density near $p=0$ does not differ significantly from LDA predictions even though the CP's do. In this vein, CP's are computed using a model 3D distribution in which free-electron spheres with appropriate weights are placed on reciprocal lattice points (extending to seven shells around a central sphere) to represent the higher momentum components in the electronic wave functions; the results show that a significant amount of

fine structure in the CP's is induced by these higher momentum components and by **k** states near the *W* points in the Brillouin zone where the free-electron spheres overlap.

The present results when compared with those reported earlier on Li show clearly that the size of discrepancies between theoretical and experimental CP's is markedly smaller in Al than in Li; in particular, theoretical and experimental profiles at $p_z=0$ differ by 16% in Li but only by 4.5% in Al, and the peak width in the second derivative at p_F is 0.23 au in Li but 0.15 au in Al. It is thus clear that, with increasing electron density, the conventional picture of the electron gas becomes more representative of the momentum density and that shortcomings of the LDA framework in describing the electron correlation effects become less important. Finally, we compare briefly our [111] CP with the positron-annihilation (1D ACAR) measurements of Okada *et al.* and show that in the case of positron annihilation the Fermi cutoff is sharper and that there is less correlation-induced smearing of structures in the ACAR spectrum.

ACKNOWLEDGMENTS

It is a pleasure to acknowledge important conversations with Bernardo Barbiellini. The Compton profile measurements were performed with the approval of the Photon Factory Advisory Committee, Proposal Nos. 92-G257, 94-G351, and 97-G288. This work is supported by the U.S. Department of Energy under Contract No. W-31-109-ENG-38 and by the Polish Committee for Scientific Research through Grant No. 2P03B02814, benefited from a travel grant from NATO and the allocation of supercomputer time at NERSC and the Northeastern University Advanced Scientific Computation Center (NU-ASCC).

[1] M.J. Cooper, Rep. Prog. Phys. **48**, 415 (1985).
[2] A. Bansil, Z. Naturforsch., A: Phys. Sci. **48**, 165 (1993).
[3] P.E. Mijnarends and A. Bansil, in *Positron Spectroscopy of Solids*, edited by A. Dupasquier and A.P. Mills, Jr. (IOS, Amsterdam, 1995), p. 25.
[4] S. Manninen, J. Phys. Chem. Solids **61**, 335 (2000).
[5] Y. Sakurai, Y. Tanaka, A. Bansil, S. Kaprzyk, A.T. Stewart, Y. Nagashima, T. Hyodo, S. Nanao, H. Kawata, and N. Shiotani, Phys. Rev. Lett. **74**, 2252 (1995).
[6] W. Schülke, G. Stutz, F. Wohlert, and A. Kaprolat, Phys. Rev. B **54**, 14 381 (1996).
[7] K. Hämäläinen, S. Manninen, C.-C. Kao, W. Caliebe, J.B. Hastings, A. Bansil, S. Kaprzyk, and P.M. Platzman, Phys. Rev. B **54**, 5453 (1996).
[8] M. Itou, Y. Sakurai, T. Ohata, A. Bansil, S. Kaprzyk, Y. Tanaka, H. Kawata, and N. Shiotani, J. Phys. Chem. Solids **59**, 99 (1998).
[9] S. Huotari, K. Hämäläinen, S. Manninen, S. Kaprzyk, A. Bansil, W. Caliebe, T. Buslaps, V. Honkimäki, and P. Suortti (unpublished).
[10] N. Shiotani, Y. Tanaka, Y. Sakurai, N. Sakai, M. Ito, F. Itoh, T. Iwazumi, and H. Kawata, J. Phys. Soc. Jpn. **62**, 239 (1993).
[11] Y. Sakurai, S. Kaprzyk, A. Bansil, Y. Tanaka, G. Stutz, H. Kawata, and N. Shiotani, J. Phys. Chem. Solids **60**, 905 (1999).
[12] G. Stutz, F. Wohlert, A. Kaprolat, W. Schülke, Y. Sakurai, Y. Tanaka, M. Ito, H. Kawata, N. Shiotani, S. Kaprzyk, and A. Bansil, Phys. Rev. B **60**, 7099 (1999).
[13] We will not concern ourselves here with questions related to uncertainties of background and core contribution in obtaining valence profiles from the Compton data, or possible breakdown of the impulse approximation at low photon energies.
[14] E. Daniel and S.H. Vosko, Phys. Rev. **120**, 2041 (1960).
[15] B.I. Lundqvist, Phys. Kondens. Mater. **6**, 206 (1967).
[16] A.W. Overhauser, Phys. Rev. B **3**, 1888 (1971).
[17] L.J. Lantto, Phys. Rev. B **22**, 1380 (1980).
[18] B. Farid, B. Heine, G. Engel, and I. Robertson, Phys. Rev. B **48**, 11 602 (1993).
[19] B. Holm and U. von Barth, Phys. Rev. B **57**, 2108 (1998).
[20] B. Kralik, P. Delaney, and S.G. Louie, Phys. Rev. Lett. **80**, 4253 (1998).
[21] C. Filippi and D.M. Ceperley, Phys. Rev. B **59**, 7907 (1999).
[22] B. Barbiellini, J. Phys. Chem. Solids **61**, 341 (2000).
[23] A.G. Eguiluz, W. Ku, and J.M. Sullivan, J. Phys. Chem. Solids **61**, 383 (2000).
[24] Y. Kubo, J. Phys. Soc. Jpn. **65**, 16 (1996).
[25] We note that Suortti *et al.* (Ref. 26) have very recently reported high-resolution Compton measurements on Al.
[26] P. Suortti, T. Buslaps, V. Honkimäki, C. Metz, A. Shukla, Th. Tschentscher, J. Kwiatkowska, F. Maniawski, A. Bansil, S. Kaprzyk, A.S. Kheifets, D.R. Lun, T. Sattler, J.R. Schneider, and F. Bell, J. Phys. Chem. Solids **61**, 397 (2000).
[27] S. Manninen, T. Paakkari, and K. Kajantie, Philos. Mag. **29**, 167 (1974).
[28] M. Cooper, P. Pattison, and B. Williams, Philos. Mag. **29**, 1237 (1974).
[29] P. Pattison, S. Manninen, J. Felsteiner, and M. Cooper, Philos. Mag. **29**, 973 (1974).
[30] D.A. Cardwell and M.J. Cooper, Philos. Mag. B **54**, 37 (1986).
[31] N. Shiotani, N. Sakai, M. Ito, O. Mao, F. Itoh, T. Iwazumi, and H. Kawata, J. Phys.: Condens. Matter **1**, SA27 (1989).
[32] Y. Sakurai, M. Ito, T. Urai, Y. Tanaka, N. Sakai, T. Iwazumi, H. Kawata, M. Ando, and N. Shiotani, Rev. Sci. Instrum. **63**, 1190 (1992).
[33] Y. Tanaka, Y. Sakurai, S. Nanao, N. Shiotani, M. Ito, N. Sakai, H. Kawata, and T. Iwazumi, J. Phys. Soc. Jpn. **63**, 3349 (1994).
[34] N. Sakai, J. Phys. Soc. Jpn. **56**, 2477 (1987).
[35] U. Von Barth and L. Hedin, J. Phys. C **5**, 1629 (1972).
[36] A. Bansil and S. Kaprzyk, Phys. Rev. B **43**, 10 335 (1991).
[37] S. Kaprzyk and A. Bansil, Phys. Rev. B **42**, 7358 (1990).
[38] A. Bansil, S. Kaprzyk, and J. Toboła, Mater. Res. Soc. Symp. Proc. **253**, 505 (1992).
[39] A. Bansil, S. Kaprzyk, P.E. Mijnarends, and J. Toboła, Phys. Rev. B **60**, 13 396 (1999).
[40] S. Kaprzyk and P.E. Mijnarends, J. Phys. C **19**, 1283 (1986).
[41] A. Bansil, S. Kaprzyk, A. Andrejczuk, L. Dobrzynski, J. Kwiatkowska, F. Maniawski, and E. Zukowski, Phys. Rev. B **57**, 314 (1998).
[42] I. Matsumoto, J. Kwiatkowska, F. Maniawski, A. Bansil, S.

Kaprzyk, M. Itou, H. Kawata, and N. Shiotani, J. Phys. Chem. Solids **61**, 375 (2000).
[43] L. Lam and P.M. Platzman, Phys. Rev. B **9**, 5122 (1974).
[44] P.E. Mijnarends, in *Compton Scattering*, edited by B.G. Williams (McGraw-Hill, New York, 1973), p. 323.
[45] M. Miasek, J. Math. Phys. **7**, 139 (1966).
[46] These are values without the Lam-Platzman correction.
[47] J. Lam, Phys. Rev. B **3**, 3243 (1971).
[48] D.M. Ceperley and B.J. Alder, Phys. Rev. Lett. **45**, 566 (1980).
[49] The difference between Al and Li based on the interacting gas computations is, however, relatively small. For example, the value of the break Z_k in the momentum density at p_F in going from Al to Li is estimated to decrease by only $\sim$10%, which would not explain the much larger observed differences pointed out in the text. Li, however, may be idiosyncratic rather than being representative of metals generally as suggested by Ref. 12.
[50] T. Okada, H. Sekizawa, and N. Shiotani, J. Phys. Soc. Jpn. **41**, 836 (1976).
[51] J. Mader, S. Berko, H. Krakauer, and A. Bansil, Phys. Rev. Lett. **37**, 1232 (1976).
[52] Y. Kubo, S. Wakoh, and J. Yamashita, J. Phys. Soc. Jpn. **41**, 830 (1976).
[53] M. Rasolt, S.B. Nickerson, and S.H. Vosko, Solid State Commun. **16**, 827 (1975).
[54] A.H. MacDonald, J. Phys. F: Met. Phys. **10**, 1737 (1980).
[55] P.E. Mijnarends, Phys. Rev. **160**, 512 (1967); **178**, 622 (1969).
[56] S. Kahana, Phys. Rev. **117**, 123 (1960); **129**, 1622 (1963).
[57] J.P. Carbotte and S. Kahana, Phys. Rev. A **139**, A213 (1965).